Springer

KSME

Journal of Mechanical Science and Technology 32 (1) (2018) 333~343
www.springerlink.com/content/1738-494x(Print)/1976-3824(Online)
DOI 10.1007/s12206-017-1233-7

Thermal simulation of machining of alumina with wire electrical discharge machining process using assisting electrode †

Meinam Annebushan Singh, Koushik Das* and Deba Kumar Sarma

Department of Mechanical Engineering, National Institute of Technology Meghalaya, Shillong, Meghalaya, 793003, India

(Manuscript Received April 19, 2017; Revised September 22, 2017; Accepted September 22, 2017)

Abstract

Electrical discharge machining or Wire electrical discharge machining have proven to be an alternate mean for machining non-conducting materials to a certain extent. Application of assisting electrode over the surface of the non-conducting material plays an important role in successful machining. A numerical model is formulated to understand the effect of assisting electrode and its thickness on material removal characteristics. The modelling is carried out for a 2-D axis-symmetric geometry using Finite element and Finite volume method. The work piece is subjected to a Gaussian distribution of heat flux through an assisting electrode layer. The thermal analysis show satisfactory results for machining of non-conducting materials by wire electrical discharge machining process. An increase in the assisting electrode thickness has resulted in higher heat dissipation rate along the radial direction as compared to the vertical depth. The developed solver has been validated with the experimental and numerical results of previous literature.

Keywords: Assisting electrode; EDM; FEM; FVM; MRR

1. Introduction

The Electrical discharge machining (EDM) / Wire electrical discharge machining (WEDM) are electro-thermal method of machining electrically conductive materials. It is a non-contact type of machining technique for complex and diverse shapes, performed using a relatively softer tool, where an intense amount of heat is focused onto a small part of the work piece. The EDM/WEDM process essentially involves generation of intense plasma between the tool and the work piece due to the generated potential difference. It is responsible for heating the work piece material at that localized position. When the temperature of the heat exposed region exceeds the melting point of the work piece material, the material gets removed either by evaporation or under the influence of the dielectric fluid. A recent advancement in the field of EDM/WEDM is the ability to machine Non-conducting materials (NCM) with the incorporation of an Assisting electrode (AE) layer [1]. Numerous works have been performed considering various NCM, AE materials and input conditions [2-4].

The knowledge of the actual working mechanism inside the EDM/WEDM process is still at large under rated. Various numerical works have been reported to analyse the actual working mechanics. Such models help predict the actual working mechanism of the machining process. Snoeys and Dijck [5], Beck [6] and Jilani and Pandey [7] considered a disk type heat source in their analysis for thermal loading condition. Dibitonto et al. [8] and Patel et al. [9] numerically modelled the cathode/anode erosion phenomena by using a single point heat source. It was observed that the point heat source model agrees with the experimentally obtained results to a better extent. For any simulation process, it is of utmost importance to understand the actual heat transfer mechanism and the condition to which the system is subjected. Dibitonto et al. [8] performed a series of experiments to identify the total fraction of heat energy that has been transferred to the work piece. It has been observed that only a normalised percentage of 18.3 % of the total heat is supplied to the work piece. This value of percentage of transferred heat to the work piece has widely been used by many researchers in various numerical models of machining process in EDM/WEDM [10-13].

Yeo et al. [14] critically analyzed and compared various numerical models [5-8, 15] and found that the model proposed by Dibitonto et al. [8] agrees best with the experimentally obtained values. The factor of the total discharge energy (Thermal energy) that reaches the work piece is a very important criteria in the numerical formulations [16]. Singh [17] has experimentally analysed the energy distribution in EDM process and concluded that the pulse duration and supplied current are the two important criteria that relates to the fraction of energy reaching the work piece. Haong et al. [18] observed

*Corresponding author. Tel.: +91 9485177054, Fax.: +91 3642501113
E-mail address: koushik.das@nitm.ac.in
† Recommended by Editor Hyung Wook Park

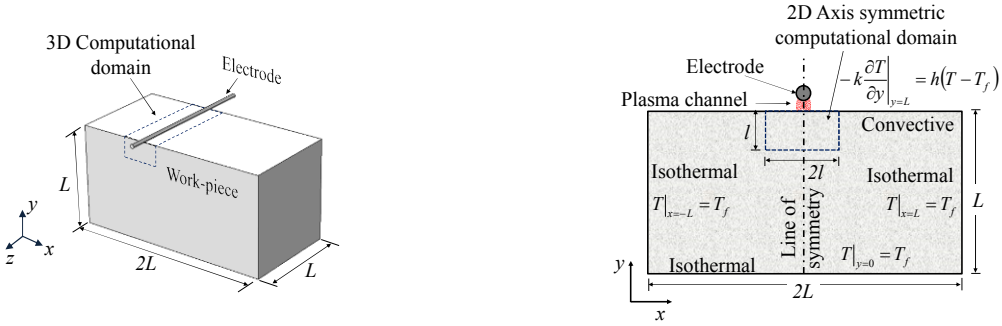

Fig. 1. Schematic of (a) 3-D model of a WEDM system along with its; (b) 2-D representation.

that the fraction of net thermal energy responsible for actual material removal is in the range of 8 – 12 % of the total discharge energy. However, this depends on the tool material, work piece material and the nature of the polarity. A relationship was established by Wuyi et al. [19] from the work of Singh [17] to investigate the total fraction of energy transferred to the work piece as a function of current and pulse on time. The results obtained were found much closer to the experimental work of Dibitonto et al. [8]. The Finite element method (FEM) [12, 13, 19, 20], the Finite difference method (FDM) [21, 22] and the Finite volume method (FVM) [23, 24] has been adopted to calculate the temperature distribution, the Material removal rate (MRR) and the surface finish (R_a). The analyses show a closer agreement with the experimental data.

Machining of NCM using EDM/WEDM [1] is a very new concept and the area is still in its initial phase. Hou et al. [25] adopted the double layer model structure to simulate the temperature distribution and the corresponding thermal stresses in WEDM. The addition of a conductive layer increases the crater volume which in turn relates to a higher MRR. In the present work, the thermal energy equation has been solved for a 2-D model of the work piece. The governing equation is discretized using FVM and the developed solver is validated against the experimental results of previous work. An FEM based commercial solver COMSOL multiphysics is utilized in the validation process. The model is formulated to identify the temperature distribution profile that has been developed during the machining of NCM in WEDM. The details of the model formulation and the obtained results are presented in this article followed by the conclusion.

2. Formulations and geometry

Schematics of a 3-D system for WEDM have been shown in Fig. 1(a). Assuming, no heat transfer in z-direction, 2-D domain of the same system can be considered in *xy*-plane (Fig. 1(b)). The left, the right and the bottom boundaries are far away from the heat affected zone and are in contact with the dielectric fluid. Due to very small size of the plasma channel, without any bulk motion of the surrounding fluid near these walls, the fluid will be maintained almost at constant temperature of T_f. Hence, all these boundaries, except the top one are at isothermal condition, T-T_f. The top boundary of the 2-D domain, closer to the plasma channel is considered convective in nature (Fig. 1(b)). In order to reduce the computational effort, the 2-D domain considered for this study is much smaller than the actual system, and is represented by dotted lines in Fig. 1(b). The computational domain is a subsystem of the actual 2-D system located at the top. Hence, except the top, all other boundaries are assumed at thermally symmetric condition (Fig. 2). In the vicinity of the plasma channel, the top boundary is subjected to a heat flux of *q"*. For computational ease, the system is further simplified by considering a line of symmetry through the vertical centerline and only the right hand side is taken into account for computation.

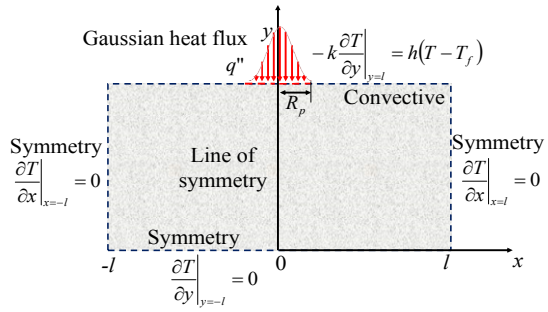

Fig. 2. Schematic of the 2-D Cartesian computational domain.

For application in a 2-D system in Cartesian coordinates, general heat conduction physics is represented by Eq. (1). The thermo-physical properties like the density (ρ), specific heat (c_p), and the thermal conductivity (k), are taken independent of temperature. In practical scenario, removal of materials is mainly by heating and erosion of sections exposed to the intense plasma. The actual removal occurs once the work piece material is above the melting point of the material.

$$\rho c_p \frac{\partial T}{\partial t} = \frac{\partial}{\partial x}\left(k\frac{\partial T}{\partial x}\right) + \frac{\partial}{\partial y}\left(k\frac{\partial T}{\partial y}\right). \quad (1)$$

In actual machining scenario, the heat flux *q"* supplied to

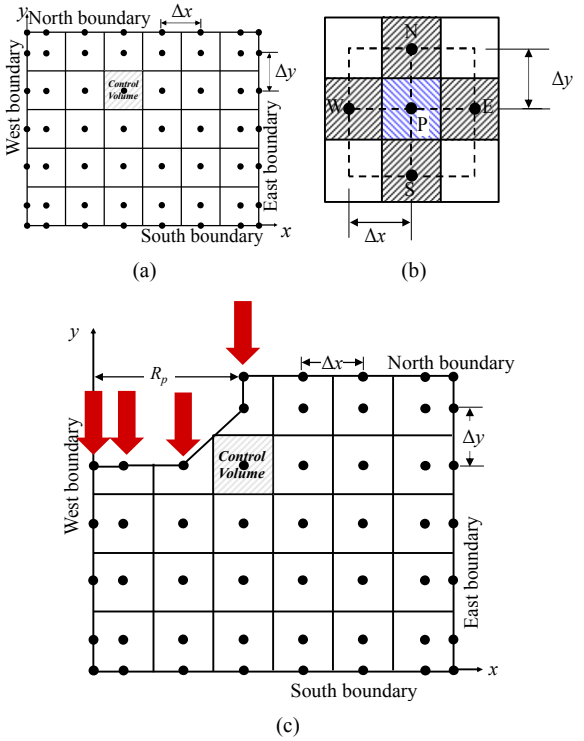

Fig. 3. Schematic of (a) 2-D discretised space; (b) control volume; (c) 2-D discretised space after time t.

the work piece surface follows a Gaussian distribution (Fig. 2). This is a major constituent in numerical simulation of WEDM process. It helps to overcome the major setbacks associated with previous work involving point [8] and uniformly distributed heat source [5]. Therefore, a Gaussian distribution of heat flux is followed in the present work, and is given by [9, 12].

$$q''(x) = q_o \exp\left\{-4.5\left(x/R_p\right)^2\right\} \tag{2}$$

where R_p is the plasma channel radius and q_o is the maximum heat flux [26], expressed as

$$q_o = \frac{4.57F_cVI}{\pi R_p^2} \tag{3}$$

where F_c, V and I are the fraction of heat transferred to work piece, discharge voltage and the supplied current.

Numerically, establishing a proper sparking zone on the surface of the work piece is an essential criterion to ensure a proper simulation process. Generally, the duration of the pulse is very small, mostly in order of micro seconds. Therefore, the experimental measurement of spark radius is practically impossible. The current work utilizes the relationship proposed by Ikai and Hashigushi [27] to calculate the spark radius, and is given by Eq. (4). This relationship (Eq. (4)) has been found to have more realistic application compared to others [11].

$$R_p = \left(2.04e-3\right) I^{0.43} t_{on}^{0.44} \tag{4}$$

where t_{on} is the pulse on time in µs.

Heat distribution factor 'F_c' is another important aspect in numerical simulation of WEDM. It gives the fraction of the total amount of heat energy that is supplied to the work piece for actual machining purpose. Wuyi et al. [19] established a Gaussian process regression (GPR) model to calculate F_c as a factor of I and t_{on}, represented as

$$F_c = 5.672 + 0.2713 I^{0.5598} t_{\text{on}}^{0.4602} . \tag{5}$$

This relationship gives results, relatively closer to experimental data [8]; and serves as an effective means to evaluate the fraction of heat transferred to work piece for various conditions. MRR and R_a can be associated with the crater volume obtained after every spark. Therefore, the crater shape that is produced at the end of every discharge is a very important criteria to calculate the nature of the surface finish and the overall MRR. A good number of works have been reported to identify the geometry of the crater. Numerically, the shape has been assumed to be hemispherical in nature [8]. Joshi [12] observed the crater cavity to be in the form of a shallow bowl with leading side on the radial direction. The relation for crater volume (mm^3) is represented as [19]

$$V_c = \frac{1}{2}\pi R_c^2 H \tag{6}$$

where R_c and H are the crater radius and the depth of the crater, respectively.

Depending upon the obtained crater volume (V_c), a theoretical MRR (mm^3/min) can be represented as [8]

$$MRR = \frac{60V_c}{t_{on} + t_{off}} \tag{7}$$

where t_{on} and t_{off} are the pulse on and off in µs.

Furthermore, the associated surface finish was numerically calculated by Salonitis et al. [28]. Mathematically, the R_a can be expressed in terms of crater radius R_c and depth H as [28],

$$R_a = \frac{1}{4}\left(1 + \frac{R_p}{R_c}\right)^2 H . \tag{8}$$

In the current work, thermal analysis of a WEDM process has been presented for application in electrically NCM. The FVM and the FEM has been used to discretise the governing equation (Eq. (1)). The developed FVM and the commercially available FEM solvers have been used to evaluate various cases of machining NCM. Following the approach of the

Table 1. Numerical validation of the FEM and FVM solver used in the present study.

Sl. No.	Parameters			MRR (mm^3/min)					R_a (μm)			
	I (A)	t_{on} (μs)	t_{off} (μs)	Dibitonto et al. [8]		Joshi and Pande [12]	Present numerical results		Dibitonto et al. [8]		Present numerical results	
				Exp. data	Num. results	Num. results	FEM	FVM	Exp. data	Num. results	FEM	FVM
1	2.34	5.6	1	0.3	13.82	12.13	4.15	4.58	1	8.28	8.97	9.79
2	2.83	7.5	1.3	1.6	17.26	16.36	3.35	6.52	1.3	9.89	9.87	13.64
3	3.67	13	2.4	3.1	21.78	20.36	6.64	8.45	1.7	12.94	14.52	14.43
4	5.3	18	2.4	8.4	35.58	34.49	13.35	18.35	2	16.76	19.27	20.18
5	8.5	24	2.4	23.2	63.79	62.86	32.61	39.34	3.2	23.51	25.99	26.26
6	10	32	2.4	32	77.18	76.37	44.19	54.0	3.5	26.50	31.25	32.81
7	12.8	42	3.2	50.5	100.33	96.68	71.29	81.45	4	33.05	39.39	41.62

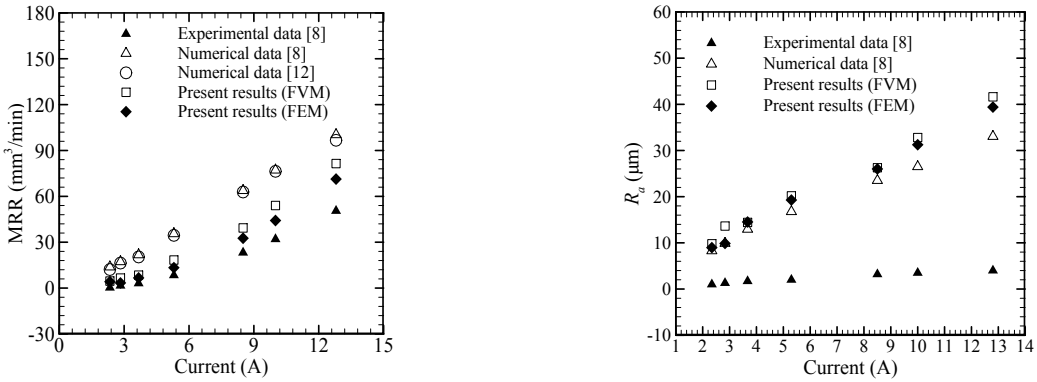

Fig. 4. Current A variation of (a) MRR with supplied current; (b) R_a with supplied current.

FVM [29], Eq. (1) is first integrated over a discrete time Δt and volume ΔV. With reference to Figs. 3(a) and (b), the discrete form of Eq. (1) with explicit approach becomes

$$T_P^{n+1} = T_P^n + \frac{\Delta tk}{\rho c_P (\Delta x)^2}\left(T_E^n - 2T_P^n + T_W^n\right) + \frac{\Delta tk}{\rho c_P (\Delta y)^2}\left(T_N^n - 2T_P^n + T_S^n\right) \quad (9)$$

where the variables with suffix P are the volume averaged values at the centre of the discrete control volume (Fig. 3(b)), and those with suffixes E, W, N and S are the same at its east, west, north and south neighboring nodes, respectively. The used scheme in the above discretization is an explicit one, the stability criterion for the same is [29]

$$\Delta t \le \left[\frac{2\alpha}{(\Delta x)^2} + \frac{2\alpha}{(\Delta y)^2}\right]^{-1}. \quad (10)$$

Solution of Eq. (9) gives a temporal distribution of temperature inside the considered domain (Fig. 2). Initially, the material is assumed to be at the surrounding temperature of T_f. The present work also follows a standard FEM formulation [12] for a 2-D geometry. In order to capture a proper material removal, the considered grid is refined near the NW-corner (Fig. 3(c)) of the domain. The numerical simulation has been carried out with the assumption that both toll and work piece are homogenous and isotropic in nature, mode of heat transfer is by conduction with 100 % plasma efficiency. Further, the model is formulated for a single spark discharge only.

3. Results and discussion

From actual experimental scenario, actual MRR and R_a is influenced by several criteria other than the input parameters. Factors such as the flushing efficiency of plasma, formation of the recast layer, the ignition and sparking delay and the dielectric fluid falls into this category. Thus, the real time scenario is very difficult to be realized in numerical simulation. In order to overcome the problem of simulating these factors and to simplify our domain, a single spark per pulse is considered for computation in the 2-D axis-symmetric plane. The solver developed using FEM and FVM is validated with the experimental and numerical data of Dibitonto et al. [8] and Joshi and Pande [12], respectively. A 2-D axis symmetric Cartesian domain of size 0.5 mm x 0.5 mm is discretised using FVM into 500 x 500 Control volumes (CV). With the boundary conditions described in the previous sections, a Gaussian heat

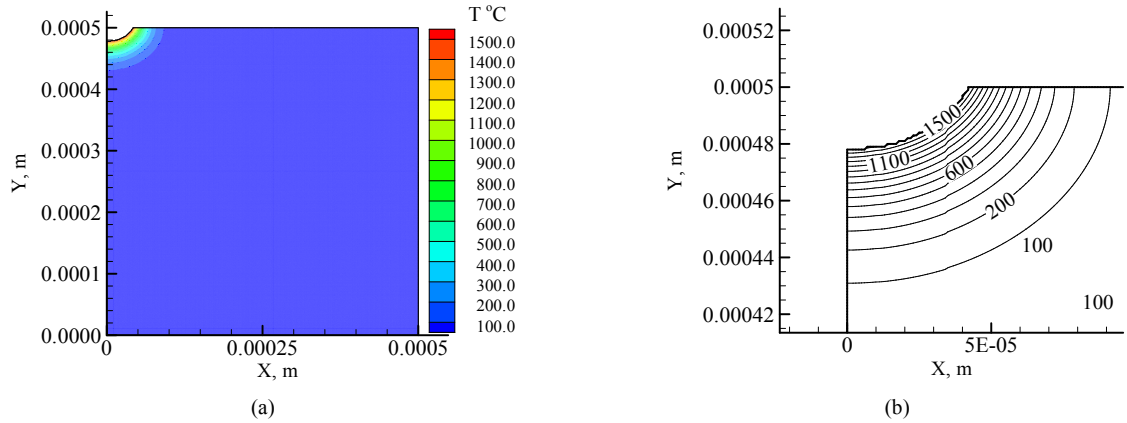

Fig. 5. (a) Temporal distribution of temperature during machining using WEDM; (b) the geometry of the crater profile.

flux of $q''(x)$ (Eq. (2)) is supplied on the North boundary over a length of R_p (Eq. (4)) (Fig. 2). For the purpose of validation, AISI W1 tool steel (T_{MP} = 1535 °C) having the thermal conductivity k = 56.1 W/m·K, the density ρ = 7545 kg/m^3 and the specific heat c_p = 575 J/kg·K has been considered with reference to Dibitonto et al. [8]. The work piece is assumed to be in contact with a fluid with temperature T_f = 25 °C and heat transfer coefficient h = 20 W/m^2·K. A voltage of 25 V is used for various cases of I, t_{on} and t_{off} as shown in Table 1. The same is further solved using FEM under the same machining conditions as mentioned in Dibitonto et al. [8]. A comparison of the MRR and R_a are summarized in Table 1, for the present results and the available literature.

It has been observed that the present numerical results of MRR are much closer to the experimental data of Dibitonto et al. [8] compared to their numerically simulated results. With minimum values of error compared to the numerical results of Joshi and Pande [12], present solvers give better accuracy in the MRR value (Table 1). During the FEM analysis, a triangular mesh with 138850 numbers of elements, with varying size, has been considered. The grid size at the *NW*-corner is refined to capture the formation of the crater with greater accuracy. Similarly, the FVM analysis has also adopted a uniformly distributed grid of size 500×500. Though a closer value of MRR has been observed between the FEM and the FVM solver, the FEM results are found to yield minimum error with the experimental data [8]. It has also been observed that the deviation of the obtained values of R_a is well within the appreciable range compared to the theoretical data laid out by Dibitonto et al. [8]. Fig. 4(a) shows a comparative analysis of the variation of MRR with the supplied current, for the cases shown in Table 1. At constant voltage, with increase in current, the rate of material removal increases. This shows the direct dependence of overall machining process as a function of current. The variations of R_a with the supplied current for the considered cases are presented in Fig. 4(b). The results obtained using FEM analysis shows a better agreement with the experimental data compared to the FVM results. Fig. 5 shows a contour of temporal distribution of temperature, along with the geometry of the formed crater, for the case no. 7 (Table 1).

For electrically conducting materials, the generated spark between the tool and the work piece is the prime source of energy for material removal. The spark generates a zone of intense plasma with high thermal energy. The thermal energy so produced heats the work-piece at the *NW*- corner ($0 \le x \le R_p$, $y = l$) and the rise in temperature will initially be experienced at location ($x = 0$, $y = l$) (Fig. 2). The thermal energy accumulated on the solid surface is dissipated in all the directions by mode of thermal conduction. Due to homogenous distribution of thermo-physical properties of the considered system, a thermal font propagates radially in all the directions, at a uniform rate. In the present analysis, consideration is given to a pulsatile heat source having temporal non-uniform behaviour. The t_{on} and t_{off} time are selected in such a way that, the rate at which the thermal energy dissipate, must be less than the rate of its accumulation over the work piece. Due to higher rate of accumulation over the rate of diffusion, the sparking zone reaches a temperature well above the melting point of the material. The molten material so formed gets removed from the work piece due to evaporation and plasma flushing. The present work considers a 100 % plasma flushing efficiency of the system. Material removed over time by this phenomenon during EDM/WEDM process results in formation of a crater.

Having validated the adopted solvers, the study has been further extended to analyse an electrically non-conducting material using WEDM process. Establishment of an initial intermitted electric spark requires an electrically conducting work piece. In the present scenario, a thin layer of conducting material is applied over the work piece to start the sparking process. Such layers of conducting materials are called AE. The use of AE helps in the initial spark formation while machining non-conducting materials. It is also expected that the presence of a highly conducting layer will affect the MRR and the surface finish of the end product. The present work considers alumina (Al_2O_3) and copper (Cu) as the work piece and the AE material, respectively. The material removal process is simulated numerically considering the thermal analysis of the

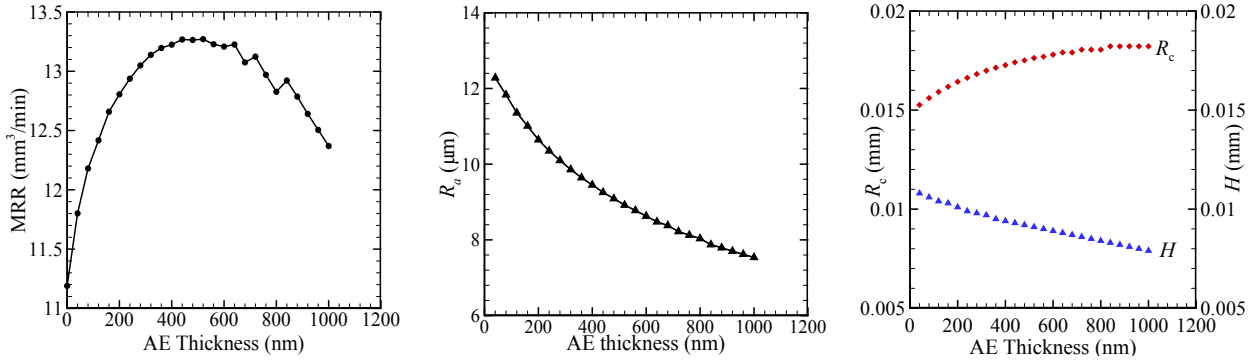

Fig. 6. Variation of (a) MRR (mm^3/min); (b) R_a (μm); (c) crater profile parameters (R_c and H) with AE thickness.

system. The results obtained from the numerical solution are used to evaluate the MRR and the surface finish. In practical scenario, there are numerous input factors that affect the performance parameters in EDM/WEDM, viz., the current, the voltage, the pulse type, the pulse on-off time, the work piece clamping positions, the nature, type and strength of dielectric fluid, the material of the electrode, etc. In the present study, the MRR and the surface finish of the end product is considered only to be affected by the current, voltage and pulse on-off time. The presence of AE is a deciding parameter in this process. Hence, a system with and without AE are taken into account for the study. It has been found that the thickness of the AE is also one of the affecting parameters of MRR. Therefore, identification of a proper AE thickness in WEDM is very important.

With work piece material considered as alumina (k = 27 W/m·K, ρ = 3900 kg/m^3, c_p = 900 J/kg·K and T_{MP} = 2057 °C) and AE material as copper (k = 400 W/m·K, ρ = 8700 kg/m^3 and c_p = 385 J/kg·K), a typical working condition has been simulated to verify the optimum AE thickness. Considering an AE layer with thickness varying from 0 nm to 1000 nm, the operating condition has been set to: voltage V = 60 V, current I = 2 A and pulse on and off time of 10 μs each, respectively. The dimension of the work piece and the operating boundary conditions are kept same as the earlier study. While calculating the MRR of the work piece material, it has been noted that with increase in thickness of the AE, the MRR increases up to a limiting value of 520 nm (Fig. 6(a)). Beyond this value, a reduction in the MRR has been observed. However, with increase in AE thickness, the surface roughness (R_a) decreases (Fig. 6(b)). Fig. 6(c) shows the variation of crater radius and the depth of the crater profile with increase in AE thickness.

Fig. 6(c) shows a decrease in the depth of the carter with increase in the AE thickness, which is expected to affect the overall Machining time (MT). Therefore to evaluate the same, the current scenario is assumed for machining of alumina over a length of $\bar{L}$ using WEDM process. For a duration of single pulse, the velocity of propagation of the tool (Wire) can be expressed as

$$v_H = \frac{c_1 H}{t_{on} + t_{off}} \tag{11}$$

where c_1 is a constant or a function which takes into account the various factors that affects the overall machinability like the tension of the wire, spark gap, flushing efficiency, wire wear, dielectric fluid strength etc. The total machining time for removal of material over a length $\bar{L}$ can be given as

$$MT_{\bar{L}} = \frac{c_2 \bar{L}}{v_H} \tag{12}$$

where c_2 is another constant or a function that takes into account various factors that affects the overall machining process. Combining the above two equation gives

$$MT_{\bar{L}} = \frac{c_2 \bar{L}\left(t_{on} + t_{off}\right)}{c_1 H}. \tag{13}$$

For a particular experimental case, length $\bar{L}$ and the pulse duration t_{on} and t_{off} will always remain fixed. Therefore Eq. (13) can be modified to have

$$MT_{\bar{L}} \alpha \frac{1}{H}. \tag{14}$$

Copper being a good conductor, application of a thin layer over the Al_2O_3 work piece facilitates higher dissipation of thermal energy due to higher span in radial direction, during the machining process. However, in the direction of machining depth, the flow of thermal energy is obstructed by the Al_2O_3 material with lesser thermal conductivity. Theoretically, with increase in AE thickness, the heat transfer surface area inside the AE increases in the radial direction. Thus, the crater radius increases with increase in AE thickness. This ultimately reduces the crater depth as more amount of heat has been dissipated in the radial direction. It has been observed that the overall machining time (MT_L) is inversely proportional to the crater depth (Eq. (14)). Therefore, with increase in AE thick-

Table 2. Effect of AE on the MRR and R_a of machining non-conducting materials in WEDM.

Case No.	V (V)	I (A)	t_{on} (μs)	t_{off} μs)	Without AE				With AE			
					R_c (mm)	H (mm)	MRR (mm^3/min)	R_a (μm)	R_c (mm)	H (mm)	MRR (mm^3/min)	R_a (μm)
1	40	2	10	10	0.0125	0.0083	6.11	11.84	0.0135	0.0071	6.09	4.03
2			25	25	0.0163	0.0100	5.01	16.79	0.0168	0.0086	4.55	5.47
3		4	10	10	0.0172	0.0106	14.74	14.81	0.0187	0.0097	15.97	5.45
4			25	25	0.0236	0.0141	14.76	21.68	0.0248	0.0130	15.05	7.81
5		6	10	10	0.0205	0.0119	23.69	16.51	0.0223	0.0111	26.10	6.24
6			25	25	0.0288	0.0164	25.70	24.51	0.0304	0.0155	26.94	9.18
7		8	10	10	0.0234	0.0128	32.92	17.65	0.0252	0.0121	36.29	6.79
8			25	25	0.0331	0.0181	37.36	26.49	0.0349	0.0173	39.57	10.13
9	60	2	10	10	0.0149	0.0109	11.32	12.79	0.0167	0.0099	12.99	5.02
10			25	25	0.0202	0.0142	10.89	18.57	0.0217	0.0130	11.49	7.13
11		4	10	10	0.0196	0.0131	23.84	15.72	0.0220	0.0123	27.93	6.34
12			25	25	0.0276	0.0182	26.13	23.33	0.0297	0.0172	28.63	9.36
13		6	10	10	0.0231	0.0144	36.25	17.42	0.0256	0.0137	42.16	7.12
14			25	25	0.0330	0.0204	41.97	26.10	0.0354	0.0196	46.13	10.66
15		8	10	10	0.0261	0.0152	48.73	18.56	0.0286	0.0146	56.07	7.65
16			25	25	0.0375	0.0220	58.17	28.03	0.0399	0.0213	63.79	11.58
17	80	2	10	10	0.0165	0.0126	16.12	13.34	0.0190	0.0117	19.89	5.61
18			25	25	0.0228	0.0171	16.67	19.54	0.0249	0.0160	18.68	8.14
19		4	10	10	0.0213	0.0148	31.63	16.29	0.0241	0.0140	38.51	6.91
20			25	25	0.0303	0.0209	36.22	24.28	0.0330	0.0201	41.1	10.32
21		6	10	10	0.0249	0.0160	46.66	17.98	0.0278	0.0153	55.76	7.67
22			25	25	0.0358	0.0231	55.76	27.07	0.0386	0.0224	62.83	11.61
23		8	10	10	0.0278	0.0169	61.55	19.12	0.0308	0.0162	72.46	8.22
24			25	25	0.0403	0.0247	75.56	28.99	0.0432	0.0240	84.24	12.51
25	120	2	10	10	0.0187	0.0150	24.63	13.94	0.0229	0.0147	36.26	6.46
26			25	25	0.0263	0.0210	27.37	20.75	0.0297	0.0199	33.03	9.35
27		4	10	10	0.0235	0.0171	44.27	17.01	0.0274	0.0164	58.08	7.57
28			25	25	0.0338	0.0247	53.21	25.48	0.0377	0.0242	64.74	11.68
29		6	10	10	0.0271	0.0182	63.13	18.71	0.0310	0.0176	79.97	8.34
30			25	25	0.0394	0.0268	78.37	28.26	0.0430	0.0260	90.66	12.81
31		8	10	10	0.0302	0.0190	81.62	19.86	0.0339	0.0185	99.88	8.89
32			25	25	0.0441	0.0282	103.3	30.16	0.0476	0.0276	117.60	13.72

ness, H decreases and hence, machining time increases. Thus, a finite increase in AE thickness will affect the overall machining duration too.

An increase in the AE thickness is observed to increase the MRR up to 520 nm, beyond which the MRR reduces. It is expected that as the MRR increases, the overall machining time (MT_L) will always reduce. However, from the above analysis the perception is not found true for the current scenario. It has also been found that the value of R_a is a square inverse function of R_c and a direct function of H (Eq. (8)). Therefore, an increase in R_c and decrease in H with AE thickness will always reduce R_a. To incorporate a higher MRR, and at the same time to ensure an optimum value of surface roughness and machining time, an optimum AE thickness needs to be selected. Hence, based on the above understandings, an AE thickness of 260 nm has been considered to perform further parametric analysis. With an optimum AE thickness of 260 nm, Table 2 shows the variation of MRR and R_a with and without AE, considering various sets of input parameters. The initial and the boundary conditions are maintained same as the previous study. The input parameters chosen for the study are voltage: 40-120 V, current: 2-8 A, and pulse on and off time: 10-25 μs. The input parameters are chosen based on the previous research work and expert opinion.

Addition of a highly conducting layer of metal over the work piece facilitates greater dissipation of heat in the x-direction. This increases the size of the machining zone in the

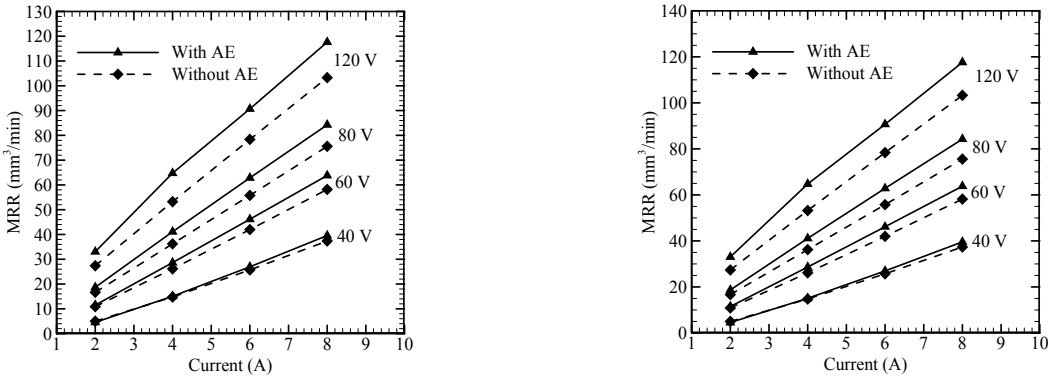

Fig. 7. Variation of MRR with current at (a) t_{on} = 10 µs; (b) t_{on} = 25 µs.

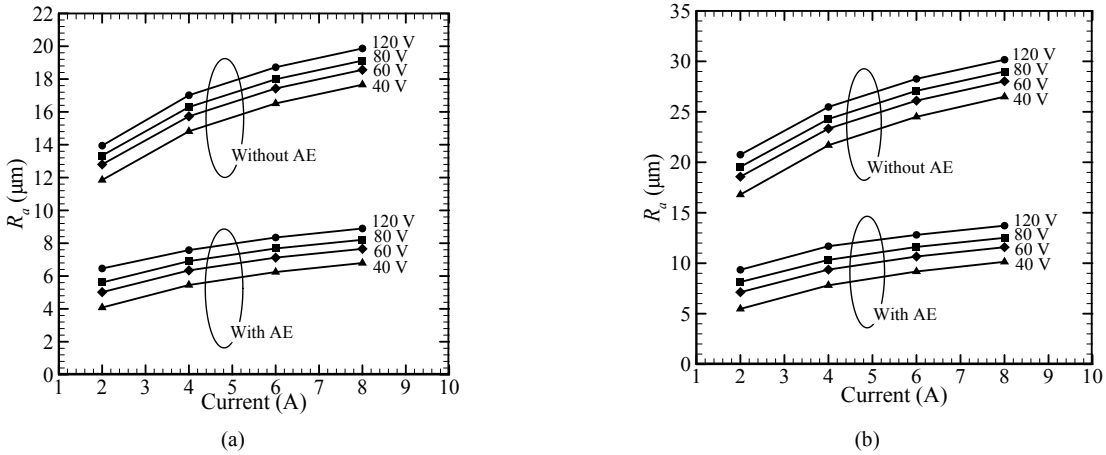

Fig. 8. Variation of R_a with current at (a) t_{on} = 10 µs; (b) t_{on} = 25 µs.

x-direction. As the amount of the supplied heat in a particular case with and without AE is the same, the amount of diffused thermal energy will be lesser in the *y*-direction for a case with AE. The amount of increment of radius of the crater has been found more than the rate of decrement of the crater depth, for the case with AE, compared to the case without AE (Table 2). Hence, the end result is an increase in the crater volume and finally the MRR. Table 2 shows the comparative values of MRR and R_a for various considered input parameters. A comparative plot of MRR with current for different values of the supplied voltage has been presented in Fig. 7. It can also be seen from Figs. 7(a) and (b) that the rate of increase in MRR with AE is much higher at higher voltage for particular pulse timing and supplied current. Thus it depicts the direct dependence of crater profile and the overall MRR to the amount of heat being supplied.

Results show that the addition of a conducting Cu layer helps to improve the R_a too (Fig. 8). It is due to the same reason for improvement in the MRR value. The R_a is an inverse quadratic function of R_c and a linear function of H (Eq. (8)). An increment in the value of R_c affects the R_a more compared to the decrement of H due to its quadratic nature. Hence, the change in the value of R_a is contributed more by the value of increment in R_c^2 rather than decrement in the value of H. Therefore, compared to the cases without AE, the obtained surface finish is better in the cases with AE. The improvement in the value of performance parameters are also realized in actual experimental scenario [30]. During machining using WEDM, the use of an AE helps in the removal of material from the work piece by combined effect of melting, evaporation, erosion and spalling rather than by spalling effect alone, in case of materials with lower thermal conductivity. Hence, improvement in these parameters are also realized in practical conditions.

The present work considers a duty factor value of 50 %. With two sets of pulse timings, 10 µs and 25 µs (Table 2), for a lower value of current (Cases 1-2, 9-10, 17-18 and 25-26), the MRR reduces with the use of AE, slightly with increase in pulse on and off time. However, it follows a reverse trend for higher values of the amount of current. For a low value of current (2 A), with lesser value of t_{on} and t_{off} time, the overall heat transferred to the work piece is small. Due to higher thermal diffusivity of the AE material, the thermal energy dissipates at a faster rate. Hence, at the end of the single pulse

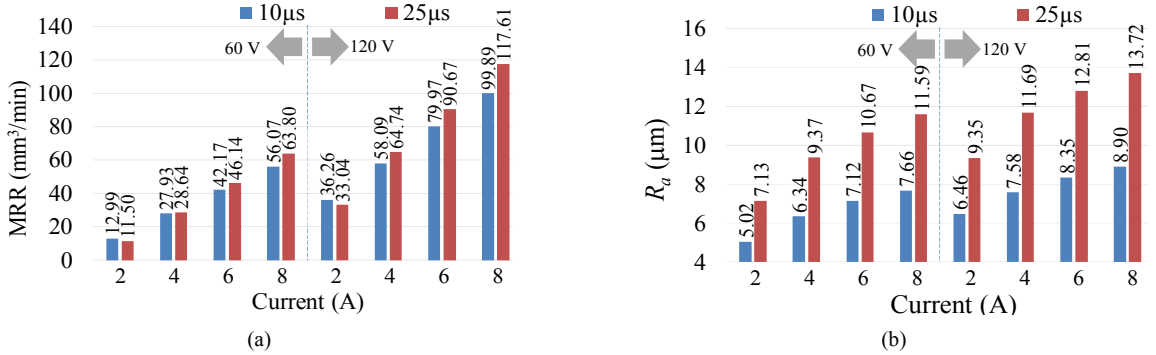

Fig. 9. Variation of (a) MRR; (b) R_a with current for machining time of 10 µs and 25 µs at voltage setting of 60 V and 120 V.

cycle, lesser amount of the work piece material reaches the melting point temperature. Thus, for lower value of current, it shows a lesser MRR for higher value of t_{on} and t_{off} time and vice-versa (Fig. 9(a)). Also, Fig. 9(b) shows the variation of R_a with pulse timing for various current. For a particular set of conditions, it can be seen that the R_a is affected by varying pulse timing, with larger pulse timing of 25 µs, the amount of material removed also increases. However, in this, the rate of increment of H is more dominating than the rate of increment of R_c. These results imply to the increase of R_a at higher pulse timing.

4. Conclusions

The present work simulates a scenario of material removal characteristics during machining of alumina in WEDM process using a conductive AE layer. The simulation is formulated based on the governing heat transfer equations and the relationships obtained from the empirical data. The developed solver is initially validated with the experimental data from the previous work. Current formulations and solvers have been found more accurate than the previous numerical studies.

An AE over the non-conducting work piece facilitates the formation of an initial spark. Presence of an AE made of Cu increases the rate of heat transfer to the work piece. However, after a critical value of AE thickness, the rate of heat transfer in the longitudinal direction starts dominating the flow of heat in the vertical direction. Hence, an increment in the crater radius and a reduction in the depth of the crater have been observed with increase in AE thickness. In the present case, the MRR has been found to have maximum value at an AE thickness of 520 nm, and further the value of MRR reduces. Due to decreasing crater depth with increase in AE thickness, the surface quality and the overall machining time are also expected to increase. Therefore, in this study, in order to achieve an optimum R_a and better machining time, an AE thickness of 260 nm has been selected for further study. Incorporation of an AE in case of non-conducting material yields a higher MRR value as compared to bare condition. It has also been found that with increase of supplied voltage and the current, MRR increases for non-conducting material. In case of alumina, with Cu as AE, at lower value of current, the MRR reduces slightly for lesser value of pulse on-off time. Also, a better surface finish was observed in such material with an AE on the work piece surface.

Nomenclature

c_p : Specific heat (J/kg·K)
F_c : Heat distribution factor
h : Heat transfer coefficient (W/m^2·K)
H : Depth of crater (mm)
I : Supplied current (A)
k : Thermal conductivity (W/m·K)
$\bar{L}$: Machining length (mm)
MT : Machining time (s)
q'' : Heat flux (W/m^2)
q_o : Maximum heat flux (W/m^2)
R_p : Crater radius (mm)
ρ : Density (kg/m^3)
T : Temperature (K)
T_f : Surrounding boundary temperature (K)
t_{on} : Pulse on time for a single spark (µs)
t_{off} : Pulse off time for a single spark (µs)
v : Tool velocity (m/s)
V : Voltage (V)
V_c : Crater volume (mm^3)

References

[1] N. Mohri, Y. Fukuzawa, T. Tani, N. Saito and K. Furutani, Assisting electrode method for machining insulating ceramics, *Ann. CIRP*, 45 (1) (1996) 201-204.

[2] J. Kozak, K. P. Rajurkar and N. Chandarana, Machining of low electrical conductive materials by Wire electrical discharge machining (WEDM), *J. Mater. Process. Technol.*, 149 (2004) 266-271.

[3] Y. H. Liu, R. J. Ji, X. P. Li, L. L. Yu, H. F. Zhang and Q. Y. Li, Effect of machining fluid on the process performance of electric discharge milling of insulating Al_2O_3 ceramic, *Int. J. Mach. Tools Manuf.*, 48 (2008) 1030-1035.

[4] Y. Guo, P. Hou, D. Shao, Z. Li, L. Wang and L. Tang,

High-speed wire electrical discharge machining of insulating zirconia with a novel assisting electrode, *Mater. Manuf. Processes*, 29 (2014) 526-531.

[5] R. Snoeys and F. S. V. Dijck, Investigation of electro discharge machining operations by means of thermos-mathematical model, *Ann. CIRP*, 20 (1) (1971) 35-37.

[6] J. V. Beck, Transient temperature in a semi-infinite cylinder heated by a disk heat source, *Int. J. Heat Mass Transfer*, 24 (10) (1981) 1631-1640.

[7] S. T. Jilani and P. C. Pandey, Analysis of surface erosion in electrical discharge machining, *Wear*, 84 (3) (1983) 275-284.

[8] D. D. Dibitonto, P. T. Eubank, M. R. Patel and M. A. Barrufet, Theoretical models of the electrical discharge machining process. I. A simple cathode erosion model, *J. Appl. Phys.*, 66 (9) (1989) 4095-4103.

[9] M. R. Patel, M. A. Barrufet and P. T. Eubank, Theoretical models of the electrical discharge machining process. II. The anode erosion model, *J. Appl. Phys.*, 66 (9) (1989) 4104-4111.

[10] L. I. Sharakhovsky, A. Marotta and A. M. Essiptchouk, Model of work piece erosion for electrical discharge machining process, *Appl. Surf. Sci.*, 253 (2006) 797-804.

[11] S. Das, M. Klotz and F. Klocke, EDM simulation: Finite element based calculation of deformation, microstructure and residual stresses, *J. Mater. Process. Technol.*, 142 (2003) 434-451.

[12] S. N. Joshi and S. S. Pande, Development of an intelligent process model for EDM, *Int. J. Adv. Manuf. Technol.*, 45 (2009) 300-317.

[13] Y. Sarikavak and C. Cogun, Single discharge thermo-electrical modeling of micromachining mechanism in electric discharge machining, *J. of Mechanical Science and Technology*, 26 (5) (2012) 1591-1597.

[14] S. H. Yeo, W. Kurnia and P. C. Tan, Critical assessment and numerical comparison of electro-thermal models in EDM, *J. Mater. Process. Technol.*, 203 (1-3) (2008) 241-251.

[15] F. S. V. Dijck and W. L. Dutre, Heat conduction model for the calculation of the volume of molten metal in electric discharges, *J. Appl. Phys.*, 7 (6) (1974) 899-910.

[16] M. Gostimirovic, P. Kovac, M. Sekulic and B. Skoric, Influence of discharge energy on machining characteristics in EDM, *J. of Mechanical Science and Technology*, 26 (1) (2012) 173-179.

[17] S. Harminder, Experimental study of distribution of energy during EDM process for utilization in thermal models, *I. J. Heat Mass Transfer*, 55 (2012) 5053-5064.

[18] K. T. Hoang, S. K. Gopalan and S. H. Yang, Study of energy distribution to electrodes in a micro-EDM process by utilizing the electro-thermal model of single discharges, *J. of Mechanical Science and Technology*, 29 (1) (2015) 349-356.

[19] M. Wuyi, G. Zhang, H. Li, J. Guo, Z. Zhang, Y. Huang and Z. Chen, A hybrid process model for EDM based on finite element method and Gaussian process regression, *Int. J. Adv. Manuf. Technol.*, 71 (2014) 1197-1211.

[20] M. Shabgard, S. N. B. Oliaer, M. Seyedzavvar and A. Najadebrahimi, Experimental investigation and 3D finite element prediction of the white layer thickness, heat affected zone, and surface roughness in EDM process, *J. of Mechanical Science and Technology*, 25 (12) (2011) 3173-3183.

[21] S. Saedodin, M. Torabi and H. Eskandar, Thermal analysis of work piece under Electrical discharge machining (EDM), using hyperbolic heat conduction model, *Majlesi J. Mech. Eng.*, 3 (4) (2010) 17-23.

[22] B. Izquierdo, J. A. Sanchez, S. Plaza, I. Pombo and N. Ortega, A numerical model of the EDM process considering the effect of multiple discharges, *I. J. Mach. Tools Manuf.*, 49 (2009) 220-229.

[23] B. Kuriachen and J. Mathew, Numerical simulation of single resistance-capacitance pulse discharge in micro electric discharge machining of Ti-6Al-4V, *I. J. Precis. Technol.*, 4 (3) (2014) 176-191.

[24] K. P. Somashekhar, S. Panda, J. Mathew and N. Ramachandran, Numerical simulation of micro-EDM model with multi-spark, *Int. J. Adv. Manuf. Technol.*, 79 (2015) 83-90.

[25] P. J. Hou, Y. F. Guo, L. X. Sun and G. Q. Deng, Simulation of temperature and thermal stress field during reciprocating travelling WEDM of insulating ceramics, *Proc. CIRP*, 6 (2013) 410-415.

[26] H. K. Kansal, S. Singh and P. Kumar, Numerical simulation of Powder mixed electric discharge machining (PMEDM) using finite element method, *Math. Comput. Modell.,* 47 (11) (2008) 1217-1237.

[27] T. Ikai and K. Hashigushi, Heat input for crater formation in EDM, *International Symposium on Electro Machining*, 11 (1995) 163-170.

[28] K. Salonitis, A. Stournaras, P. Stavropoulos and G. Chryssolouris, Thermal modeling of the material removal rate and surface roughness for die-sinking EDM, *Int. J. Adv. Manuf. Technol.*, 40 (2009) 316-323.

[29] V. K. Versteeg and W. Malalasekera, *An introduction into computational fluid dynamics,* Pearson Education Limited (2015).

[30] T. Saleh, R. N. Rasheed and G. A. Asan, Experimental study on improving μ-WEDM and μ-EDM of doped silicon by temporary metallic coating, *Int. J. Adv. Manuf. Technol.,* 78 (9) (2015) 1651-1663.

Meinam Annebushan Singh is a Research Scholar in Department of Mechanical Engineering, NIT Meghalaya, India. His area of research is in experimental and numerical analysis on non-conventional machining techniques with a focus on machining of ceramics. He has four papers in his credit.

Koushik Das is currently a Professor in the Department of Mechanical Engineering, NIT Meghalaya, India. His research domain mainly focuses on heat transfer and fluid flow characteristics. There are more than 10 research publications to his credit. He is a reviewer of Journal of Thermal Biology and Applied Mathematical Modelling.

Deba Kumar Sarma is a Professor and Associate Dean (Planning & Development), NIT Meghalaya, India. His research interest are in the field of machining design and manufacturing, application of soft computing technique in machining and non-conventional machining processes. He has published nine international journals and eight paper in international conference proceedings.